JOURNAL OF VIROLOGY, Oct. 2006, p. 9544–9556 Vol. 80, No. 19
0022-538X/06/$08.00+0 doi:10.1128/JVI.00668-06

Delayed Biosynthesis of Varicella-Zoster Virus Glycoprotein C: Upregulation by Hexamethylene Bisacetamide and Retinoic Acid Treatment of Infected Cells

Johnathan Storlie, Wallen Jackson, Jennifer Hutchinson, and Charles Grose*

Departments of Microbiology and Pediatrics, University of Iowa College of Medicine, Iowa City, Iowa 52242

Received 3 April 2006/Accepted 11 July 2006

In the course of examining the trafficking pathways of varicella-zoster virus (VZV) glycoproteins gE, gI, gH, and gB, we discovered that all four are synthesized within 4 to 6 h postinfection (hpi) in cultured cells. Thereafter, they travel via the trans-Golgi network to the outer cell membrane. When we carried out a similar analysis on VZV gC, we observed little gC biosynthesis in the first 72 hpi. Further examination disclosed that gC was present in the inocula of infected cells, but no new gC biosynthesis occurred during the first 24 to 48 h thereafter, during which time new synthesis of gE, gH, and major capsid protein was easily detectable. Similarly, delayed gC biosynthesis was confirmed with three different VZV strains and two different cell lines. Bioinformatics analyses disclosed the presence of PBX/HOX consensus binding domains in the promoter/enhancer regions of the genes for VZV gC and ORF4 protein (whose orthologs transactivate gC in other herpesviruses). Bioinformatics analysis also identified two HOXA9 activation regions on ORF4 protein. Treatment of infected cultures with chemicals known to induce the production of PBX/HOX transcription proteins, namely, hexamethylene bisacetamide (HMBA) and retinoic acid, led to more rapid gC biosynthesis. Immunoblotting demonstrated a fivefold increase in the HOXA9 protein after HMBA treatment. In summary, these results documented that gC was not produced during early VZV replication cycles, presumably related to a deficiency in the PBX/HOX transcription factors. Furthermore, these results explain the apparent spontaneous loss of VZV gC in some passaged viruses, as well as other anomalous gC results.

Varicella-zoster virus (VZV) is a very cell-associated virus in cell culture. In addition, the infectivity titers are extremely low, usually less than 1,000,000 U per 25-cm^2 monolayer. Further, the virions produced in cell culture have an aberrant appearance. Explanations for these observations are a subject of continuing research. To this end, we have been investigating the biosynthesis and maturation of several VZV structural glycoproteins found in the envelope of the virion, especially the predominant gE/gI complex. These two glycoproteins are synthesized in the Golgi and then traffic through the trans-Golgi network en route to the outer plasma membrane within the expected 12-h replication cycle of an alphaherpesvirus. After endocytosis via their tyrosine- and dileucine-based motifs, they travel back to the trans-Golgi network (12). At this location, the glycoproteins appear to be incorporated into the virion assembly vacuoles. Two other major VZV glycoproteins, gH and gB, have similar endocytosis motifs and similar trafficking profiles.

During the glycoprotein trafficking studies, VZV gC was used as a control because there are no obvious trafficking motifs in its short cytoplasmic tail (20). There have been clues that gC is important for virion production. The severe combined immunodeficient (SCID) mouse has become an important animal model for the investigation of VZV pathogenesis. In this model, implants of fetal human skin are inserted under the skin of the SCID mouse. Subsequently, the skin is injected with virus and harvested every 7 days for 21 days. Typical wild-type virus causes an infection that resembles the pathology observed with human chickenpox. Of interest, variant varicella virus not expressing gC was not able to replicate well in the skin (25). Further, these viruses failed to form prototypical virions. Little is known about gC trafficking patterns in the infected cell. Earlier reports have suggested that VZV grown in cell culture can spontaneously lose its ability to produce gC even though the virus still retains the gC gene (ORF14) (18). For the above reasons, we decided to reexamine gC biosynthesis and trafficking.

In our initial experiments, gC production was often not detected in monolayers infected with strains known to harbor an intact gC gene. In turn, this unexpected observation led us to investigate in detail the biosynthesis of gC during a typical cell culture experiment. The results presented below show a delayed pattern of gC expression that could not have been predicted based on current information about gC from other alpha herpesviruses. The same results provide evidence that PBX/HOX transcription factors, previously unknown contributors to the VZV replication cycle, are likely to be required for production of true late genes such as VZV gC. PBX/HOX transcription factors play essential roles in both human organ development and oncogenesis. These same factors may explain unusual aspects of VZV pathology in humans.

MATERIALS AND METHODS

Viruses and cells. VZV-32, VZV-Ellen, and VZV-MSP are well-known VZV strains. The complete sequence of VZV-MSP has been published (14). All strains were propagated and passaged in human melanoma cells (Mewo) in minimal essential medium supplemented with 8% fetal bovine serum and Penstrep (Invitrogen) antibiotics. VZV-32 was also grown in Vero cells. VZV-32 and VZV-MSP strains are low-passage isolates, whereas VZV-Ellen is a high-passage

* Corresponding author. Mailing address: University Hospital/2501 JCP, 200 Hawkins Dr., Iowa City, IA 52242. Phone: (319) 356-2270. Fax: (319) 356-4855. E-mail: charles-grose@uiowa.edu.

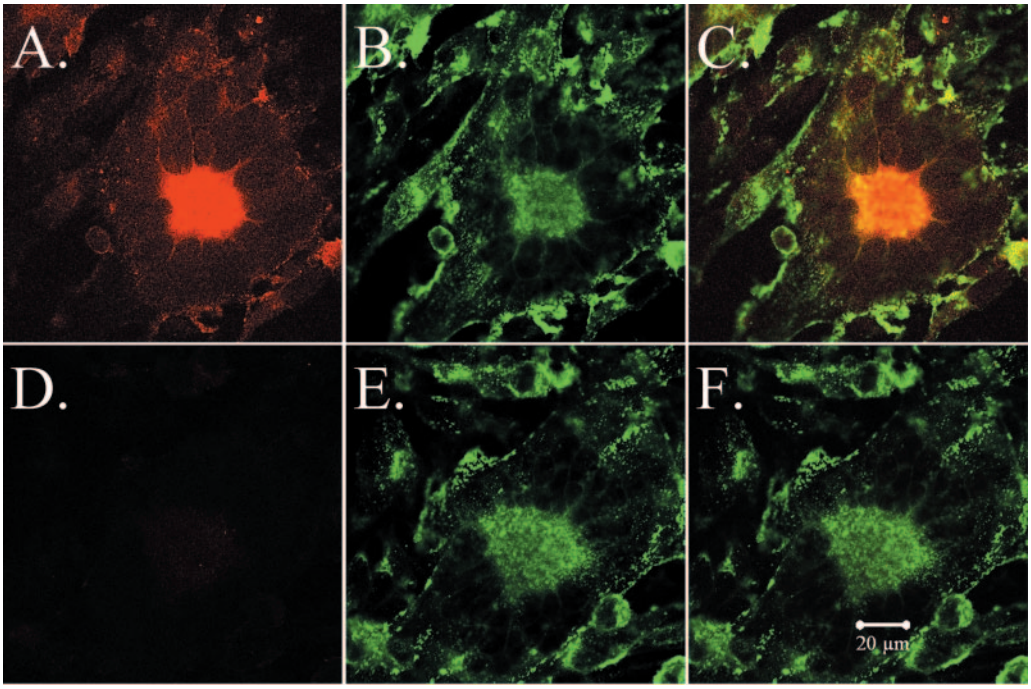

FIG. 1. VZV gC and gE expression at 48 hpi in infected cells. Imaging was carried out by confocal microscopy, using a murine MAb against gC (233) and a human MAb against gE. One syncytium showed gC immunoreactivity (A and C), while another syncytium showed no evidence of gC production (D and F). In contrast, gE was detected in both VZV-induced syncytia (B, C, E, and F). Colocalization of gC and gE is marked by the yellow color in the central area of the syncytium in panel C.

strain (>90). Infected cell monolayers used for inocula were harvested 3 to 5 days postinfection, when they showed >70% cytopathic effect (CPE). When infected monolayers were sonically disrupted, the cells were first resuspended in 2 ml of medium in a 15-ml conical tube. After sonication, each new monolayer was simultaneously inoculated with an aliquot of infected cells equivalent to one-sixth of area to be infected. These conditions of infection are similar to those previously described (13).

Treatments of VZV-infected monolayers. At the time of infection in some experiments, cells were subjected to one of the following six treatments: (i) control medium alone; (ii) retinoic acid (RA) in medium; (ii) hexamethylene bisacetamide (HMBA) in medium; (iv) RA and cortisol in medium; (v) HMBA and cortisol in medium; or (vi) RA, HMBA, and cortisol in medium. The RA concentration was 0.01 mM, the HMBA concentration was 5 mM (29, 45), and cortisol levels were 1 μM. In initial experiments, stock solutions of RA and cortisol were dissolved in dimethyl sulfoxide, with a final concentration of 0.3% dimethyl sulfoxide. Subsequent experiments substituted culture medium as the solvent for the treatments.

Confocal microscopy imaging experiments. Antibody probes included the following reagents: mouse monoclonal anti-gC antibody (MAb) clone 233, rabbit monospecific anti-gC antibody, mouse anti-gH MAb clone 258, human anti-gH MAb Ti-57, mouse anti-gE MAb clone 3B3, human anti-gE MAb V_2, mouse anti-major capsid protein (MCP; p155) MAb, and mouse anti-IE62 MAb. Most antibodies were produced in this laboratory by published techniques (11, 27) except for the the anti-MCP antibodies, which were obtained from either Advanced Biotechnologies or U.S. Biologicals, and the human MAbs were a generous gift from K. Shiraki (40). Murine MAb to HOXA9 protein was obtained from Abnova. Secondary fluoroprobes included goat anti-rabbit 488, goat anti-mouse 546, and goat anti-human 633 antibodies from Molecular Probes. Immunofluorescent images were generated by using a Zeiss LSM 510 confocal microscope at five different magnifications: ×10, ×20, ×40, ×64, and ×100. For the imaging of untreated and treated cells, all cells were fixed and permeabilized by using 0.05% Triton X-100 in 2% paraformaldehyde.

Western blotting. VZV-infected cell lysates were harvested from flasks incubated for 24, 48, 60, 72, 84, and 96 h postinfection (hpi). The monolayers were harvested and antigens prepared for immunoblotting by described techniques using SuperSignal chemiluminescent substrate (34). The samples were separated on an 8% acrylamide gel, transferred to a membrane, and blotted by using MAb 3B3 to gE and MAb 233 to gC.

RESULTS

Delayed gC expression in early VZV-induced syncytia. As an alphaherpesvirus, VZV has a 12- to 16-h replication cycle. In the initial experiments, the inoculum consisted of trypsin-dispersed infected cells from a monolayer with advanced CPE. Because the titer of input virus is so low, however, several replication cycles are required before CPE is visible in the newly infected monolayers. While examining glycoprotein expression at increasing intervals postinfection, we observed that all syncytia at early time points (24 and 48 hpi) were clearly labeled with a MAb against gE, but only an occasional VZV induced syncytium was labeled with anti-gC antibody (Fig. 1). Since the inoculum consisted of trypsinized infected cells, input syncytia were destroyed; therefore, the syncytia seen in Fig. 1 were the result of new virus replication. The center of each newly formed syncytium includes an aggregation of Golgi; thus, the newly synthesized gC protein in a positive syncytium was located mainly in Golgi (Fig. 1). Even though conditions of cell-associated VZV infection are asynchronous, by 48 hpi all input viral populations would have undergone three to four replication cycles. In all our prior studies of VZV glycoproteins, there was no precedence for the absence of gC biosynthesis this late in the infectious cycle.

To further investigate the expression of gC compared to gE over time, we infected six replicate monolayers and harvested them over a 96-h time period. When examined by immuno-

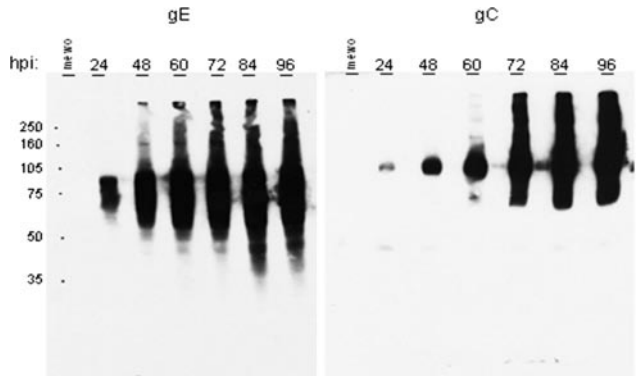

FIG. 2. Immunoblotting for VZV glycoproteins gE and gC. Infected cultures were harvested at increasing intervals after inoculation with trypsin-dispersed infected cells. Each well was loaded with an equal volume of VZV-32 lysate harvested at the hours postinfection indicated above each lane. The expected molecular mass of mature gE is 98 kDa, although several lower- and higher-molecular-mass forms have been described. The expected molecular mass of mature gC is 105 kDa; again, both lower- and higher-molecular-mass forms have been described. The MeWo lane represents the negative (uninfected) control cell lysate.

blotting, this experiment showed that gC expression was markedly delayed compared to gE (Fig. 2). Abundant amounts of gC were not observed until 72 hpi. This time point is equivalent to five to six replication cycles. Western blotting showed that gE was present in abundance at early times postinfection, whereas gC was not present in comparable amounts until about 60 hpi. Finally, in order to eliminate the possibility that gC was actually being expressed at earlier time points but not in a form recognizable by the anti-gC MAb, we generated a rabbit polyclonal monospecific anti-gC antibody; the results were comparable. The latter result indicated that weak affinity of the anti-gC MAb was unlikely to be an explanation for the immunoblotting data.

Three-dimensional reconstruction of glycoprotein gC labeled VZV-infected cells. In order to demonstrate that the expression and localization of gC were not simply outside of the plane of our original confocal images, we obtained multiple serial images of our infected cells at various time points. We also included antibody probes for other VZV proteins such as gE, gH, and major capsid protein (MCP; ORF40). This se-

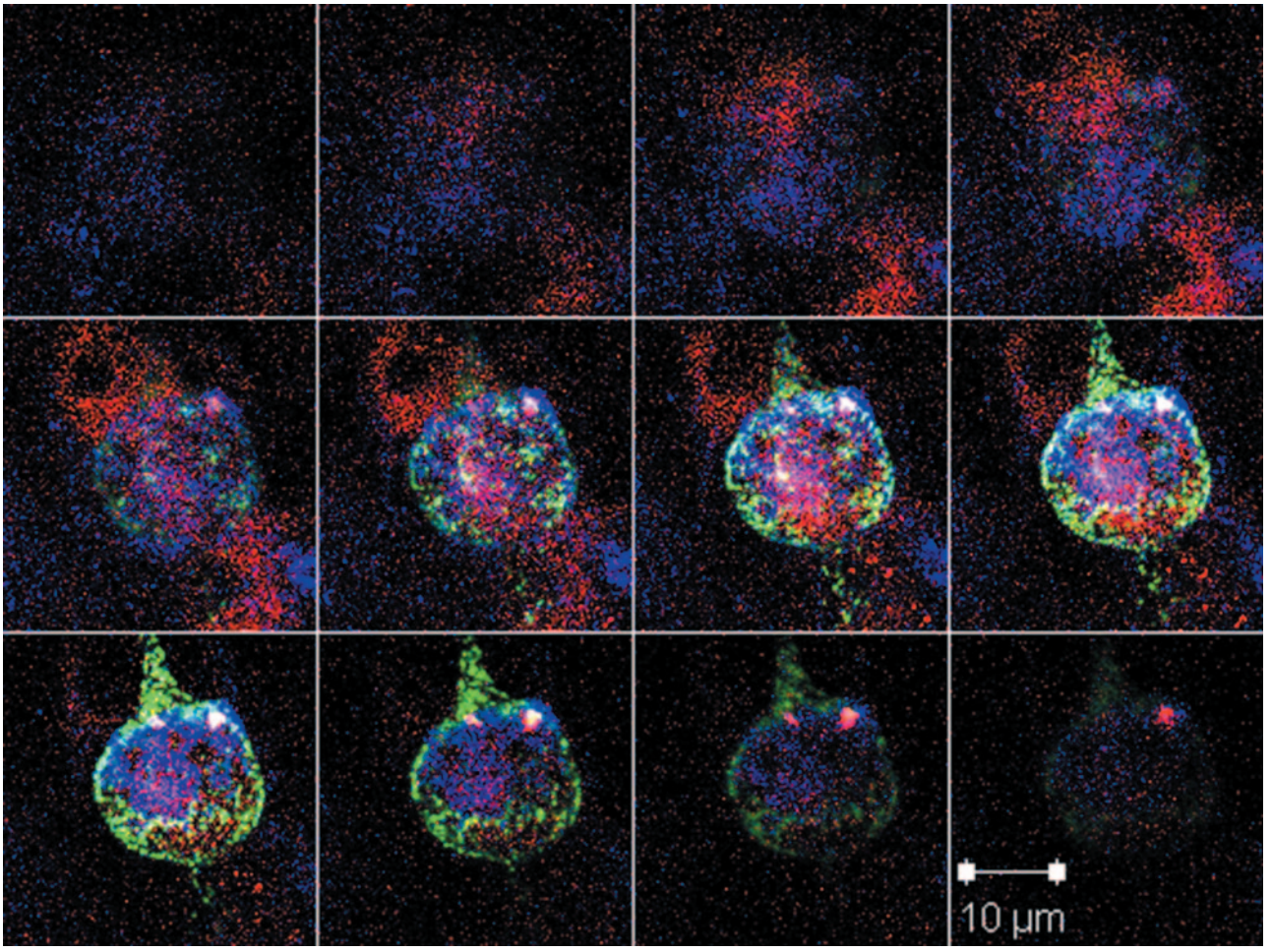

FIG. 3. Inoculum cells after trypsin dispersion of an infected monolayer. Inoculum cells were easily identified because they were a substantial source of positive gC labeling at early time points postinfection. Z-stack confocal microscopic imaging showing a rounded inoculum cell on the surface of a newly infected monolayer. The series was taken at increments of 0.5 μm. Blue, human anti-gE MAb; green, rabbit anti-gC antibody; red, murine anti-MCP MAb. The gC glycoprotein was present in abundant amounts on the surface of the inoculum cell. Careful examination of the monolayer beneath the plane of the inoculum cell at 24 hpi clearly demonstrated newly synthesized gE and MCP but no new gC.

quence of optical sections collected at different levels perpendicular to the optical axis (Z-stack) was further processed into a three-dimensional representation of the infected cell using three-dimensional projection options for ImageJ and the LSM image browser. By examining infected monolayers between 4 and 24 hpi, we were able to identify similar dense cells staining strongly for gC on the surface of the monolayer (Fig. 3). Since gC is a true late protein, cells containing abundant gC at 4 hpi could not represent newly infected cells; instead, they were cells present in the inoculum taken from a monolayer with advanced CPE. These reconstructed three-dimensional images were invaluable in demonstrating that the cells containing gC also contained other late proteins such as gE and MCP. Another point is illustrated by Fig. 3. Below the plane of the inoculum cell, there were clearly immunoreactive sites in the monolayer for both gE (blue) and MCP (red), but none for gC (green). The blue and red staining represented new formation of gE and MCP proteins as part of the first cycle of replication in the newly infected monolayer, before the appearance of CPE. The absence of gC staining confirmed the above observations that gC biosynthesis was delayed. In addition, the diameters of these structures suggested that many were singly infected cells, some with extensions attaching to the uninfected monolayer.

As an additional imaging experiment, cells were examined by immune scanning electron microscopy (SEM) (Fig. 4). When anti-VZV gC antibody was combined with a gold-labeled secondary antibody, gold beads were clearly seen on the an inoculum cell and its extensions in a pattern very similar to that observed by confocal microscopy in Fig. 3. At least 12 gold beads were present on the inoculum, and an additional two clusters were seen on an extension (14 arrowheads). A few gold beads were scattered on the monolayer. These may represent the attachment of antibody to small remnants of trypsin-dispersed infected tissues adherent to the monolayer and also seen by confocal microscopy at 24 hpi. A control infection incubated with a gold-labeled secondary antibody alone lacked any attached beads on inoculum cell or monolayer (as indicated by SEM [not shown]).

Temporal appearance of gC in infected cultures. The reconstruction experiments strengthened our conclusions that gC was present in the inoculum but was not detected during the initial cycles of replication. We next sought to establish more precisely when newly synthesized gC first appeared in infected cells. For these studies we carried out extensive confocal microscopic analyses of VZV-infected cells at daily intervals from 24 to 120 hpi. We performed experiments using both the traditional infected cell inoculum and what has been termed cell-free virus. Cell-free virus is a sonically disrupted infected cell monolayer (13). When an infected cell inoculum was examined, gC expression was first observed reliably between 48 and 72 hpi. From 96 to 120 hpi, the percentage of gC-positive syncytia increased substantially. When a sonicated virus inoculum was used, the series of events was similar but delayed a further 24 h (Fig. 5). The small amount of gC staining at 48 h was not located in the endoplasmic reticulum or Golgi and therefore represented remnants of input inoculum. In other words, gC production was not seen in the majority of syncytia until 72 to 96 hpi. Even though the syncytia in Fig. 5 showed abundant amounts of gC at 96 hpi, syncytia lacking gC were easily located in the same monolayer. In these microscopy experiments, rabbit ant-gC antibody was the probe to detect gC. Therefore, the lack of gC staining cannot be explained by a gC form lacking the epitope defined by the anti-gC MAb.

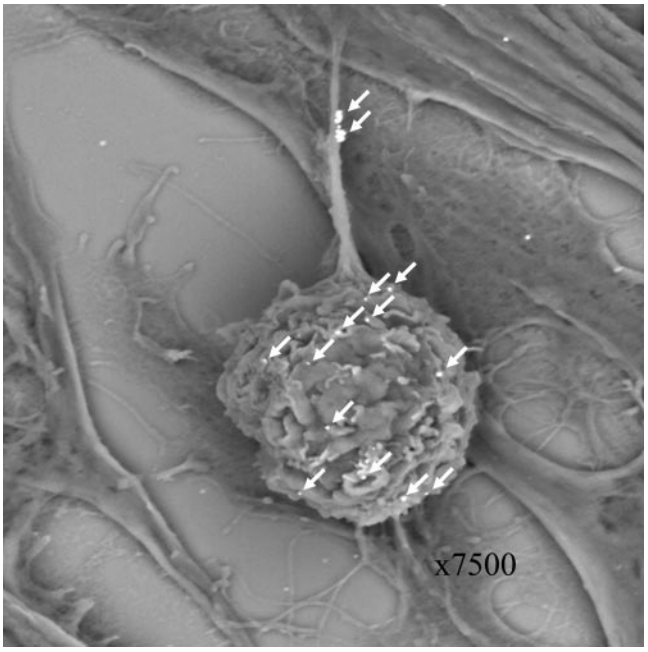

FIG. 4. Scanning electron micrograph of an inoculum cell. At 24 hpi, an infected monolayer was examined by scanning electron microscopy. The sample had been treated with a murine anti-gC MAb, followed by an immunogold-labeled anti-mouse antibody. After silver enhancement, 12 gC-positive beads were clearly seen on the surface of the inoculum cell, and two clusters of beads were observed on an extension (arrows). Compare this with the gC immunostaining in Fig. 3.

For all of these gC experiments, the positive controls included antibody probes for two of the following four VZV proteins: the regulatory IE62 protein and the three structural proteins gE, gH, and MCP. Because of the availability of antisera to these proteins produced in different species (mouse, human, and rabbit), we were able to simultaneously examine the expression of three different VZV proteins in the same experiment. IE62 was invariably present in all newly infected monolayers. Likewise, both gE and MCP were easily detectable within the earliest syncytia seen in a newly infected culture. (The IE62 and gH immunostaining experiments are not shown.) In summary, these results demonstrated that gC was not detectable during the first cycles of VZV replication and therefore was not required for formation of the typical CPE seen in VZV-infected cells.

Analyses with other cell lines and VZV strains. Two possible explanations for the effect described above needed to be excluded. First, we investigated whether the effect was specific to one VZV strain. Our initial experiments were performed with the VZV-32 strain used in this laboratory for many years (10). This strain has now been completely sequenced and contains an intact genome with no major genetic changes compared to VZV Dumas (C. Grose and G. Tipples, unpublished data). We also examined gC expression after infection of cells with two additional strains, including VZV-MSP and VZV-Ellen. VZV-

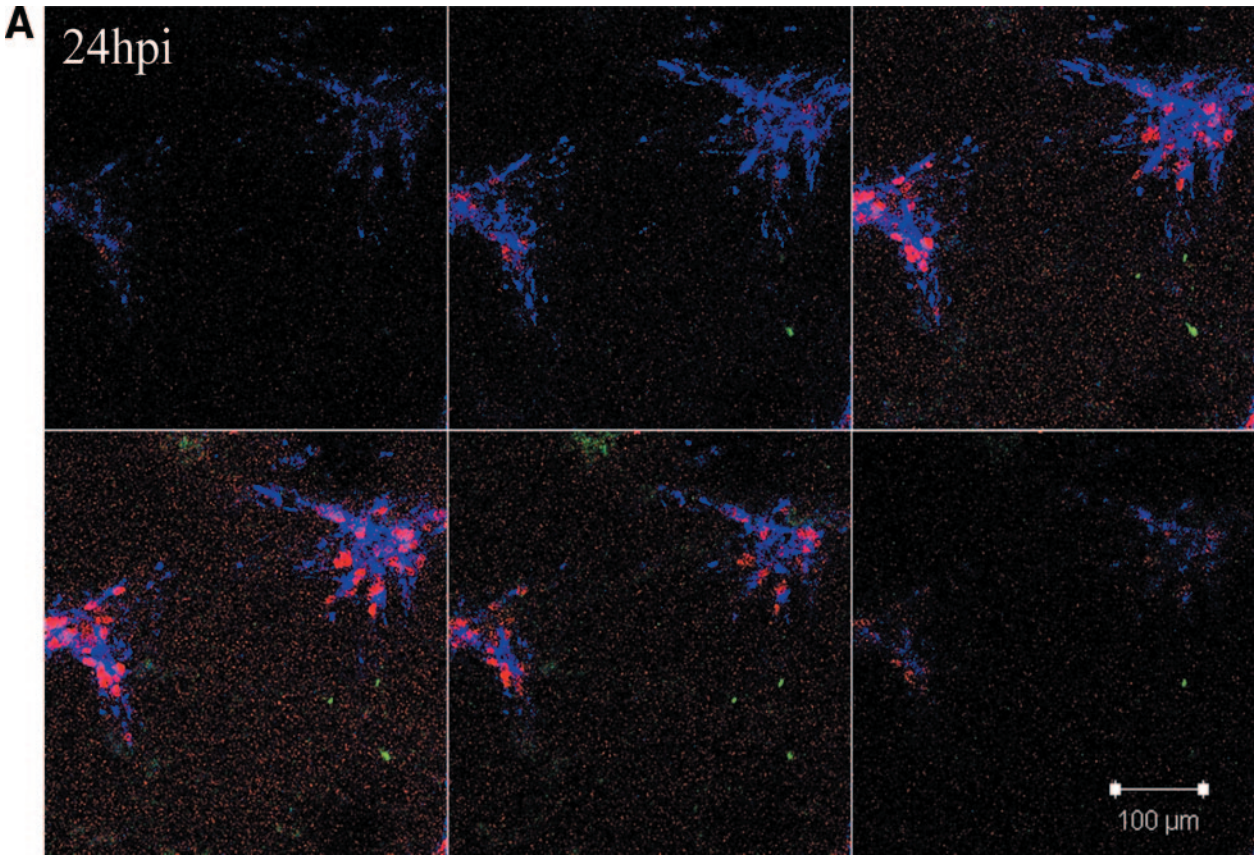

FIG. 5. Delayed expression of VZV gC in cultured Mewo cells. Mewo cells were inoculated with a sonicated VZV-infected cell lysate. Cultures were examined at 24 (A), 48 (B), 72 (C), and 96 (D) hpi by confocal microscopy, and Z-stack images were obtained for each syncytium using identical settings. Scale bars for the 24-hpi Z-stacks are applicable for all images. The panel for each time point contains six 1-μm slices of a representative area of the slide at 3.9-μm increments from the bottom to the top of the monolayer. Panels represent the four time points at 24, 48, 72, and 96 hpi. Antibody probes were the same as in Fig. 3: green, gC; blue, gE; red, MCP.

MSP has also been completely sequenced and found to have an intact gC gene. The results with the latter two strains demonstrated a delayed gC biosynthesis similar to VZV-32 strain. Second, we investigated whether the effect was specific to one cell line. Our initial experiments were performed in human melanoma cells, a substrate highly susceptible to VZV infection (15). To this end, we infected simian-derived Vero cells and found that gC production was similarly delayed (Fig. 6). In short, the marked delay in gC biosynthesis in VZV-infected cells was not restricted to one VZV strain or one cell line.

Transcription factor binding domains in VZV gC gene and ORF4. The VZV gC literature is replete with examples of variable gC expression (18–20, 25, 28). When the literature as well as our results were considered, we postulated that there was a factor associated with VZV gC expression often found in suboptimal amounts in the newly infected cell. Only when critical amounts of this factor accumulated was gC synthesized. Based on an examination of the HSV-1 literature, a possible candidate was VZV ORF4 protein, the ortholog of the regulatory HSV-1 protein ICP27. HSV ICP27 is absolutely required for maximal biosynthesis of HSV-1 gC. To this end, a bioinformatics analysis was carried out to locate potential transcription factor binding sites in both ORF14 and ORF4. MotifFinder analysis found two HOXA9 activation motifs in the ORF4 protein (IE4) (Table 1). Because one possible explanation for a delay in ORF14 transactivation could be due to a delay in ORF4 expression, we also analyzed the ORF4 promoter/enhancer regions. MatInspector analysis (2) of the promoter/enhancer regions of VZV genes ORF4 and VZV gC gene (ORF14) revealed that both contained HOXA9-binding domains and other PBX/HOX-related domains (Table 2). Of note, a HOXC13 *cis* element was found at position 17 to 1 upstream of the start site for gC.

Treatment of infected cells with RA and HMBA. Given the bioinformatics information, we postulated that increasing PBX/HOX levels would increase gC production, either directly or through increasing ORF4 protein levels. As a preliminary test of this hypothesis, we selected treatments that have been shown to upregulate PBX and HOX transcription factor expression (30–32, 36, 39). The chemicals involved in those treatments are RA, HMBA, and cortisol. The results demonstrated that both RA and HMBA treatments promoted an earlier expression of gC, which was detected at least 24 h before its appearance in nontreated cells (Fig. 7). The addition of cortisol appeared to augment RA treatment but was less effective when it accompanied HMBA. Again, the experiments were carried out at 24-h incremental time points, and the infected cells were immunolabeled simultaneously with antibodies to

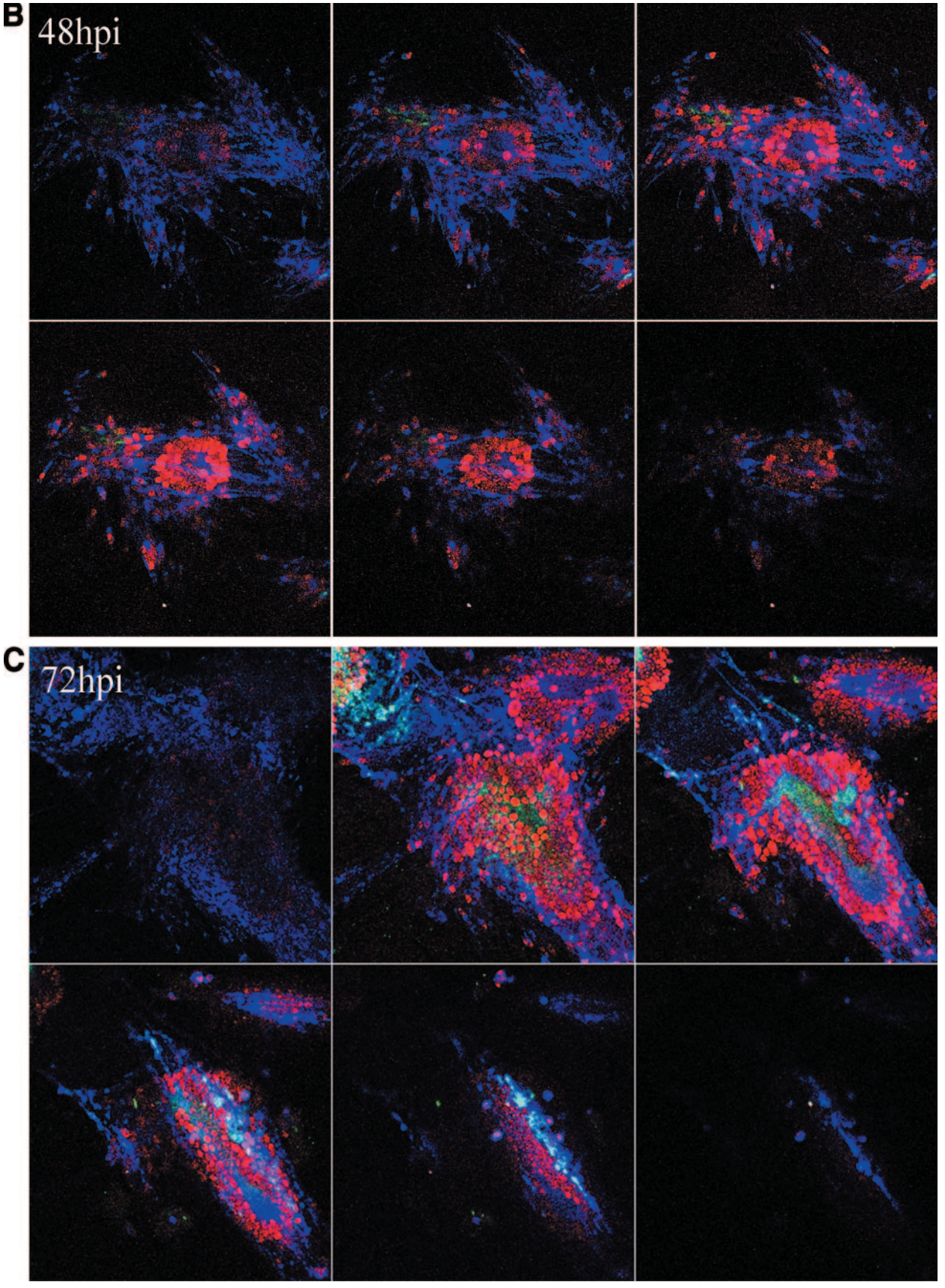

FIG. 5—*Continued.*

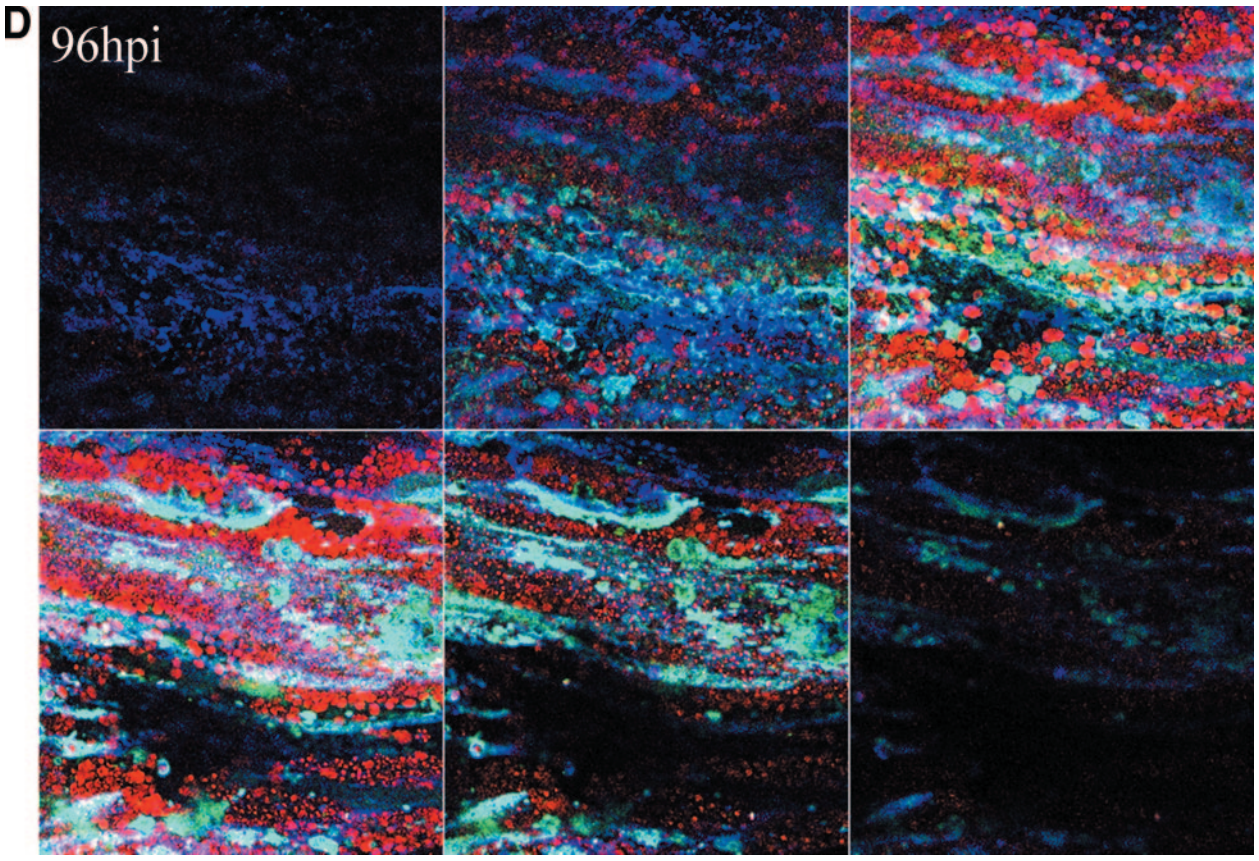

FIG. 5—*Continued.*

three different VZV proteins. The samples were analyzed after the capture of multiple images in a Z-stack to assure that VZV proteins in every plane of the infected monolayer were detected. The results clearly showed that gC production was detectable 24 h earlier in infected cells treated with either RA or HMBA (compare the green in panels at 48 and 72 hpi).

As a final means to document the specificity of the increased gC synthesis after treatment, we quantified the differences in glycoprotein expression under each of the conditions described above. The relative amounts of gC, gE, and MCP present at the given time points after each treatment were measured by quantifying the fluorescence of each immunolabeled protein on images generated under otherwise identical conditions using identical confocal settings for all time points. ImageJ RGB measure (available from the National Institutes of Health) was used to precisely identify the relative levels of the three immunolabels. The ratio of VZV gC to gE production increased at both 48 and 72 hpi with treatment (Fig. 8). This increase in the

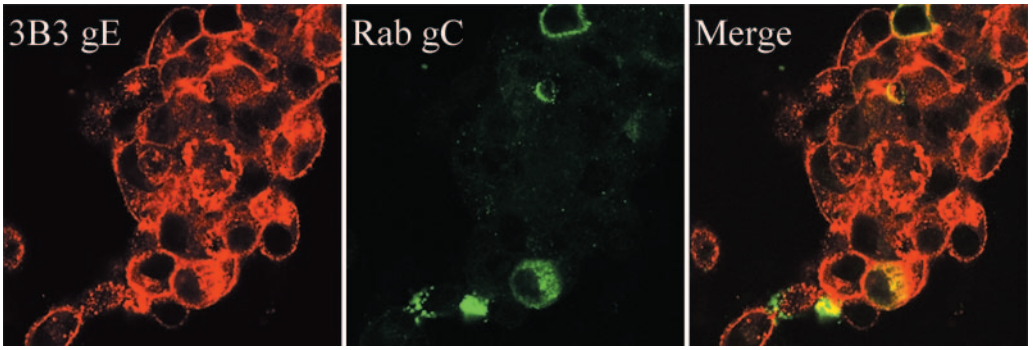

FIG. 6. Delayed expression of VZV gC in cultured Vero cells. Vero cell monolayers were inoculated with cells prepared from a trypsin-dispersed VZV-infected Vero cell monolayer with advanced CPE. Cultures were examined at 24, 48, 72, and 96 hpi, after immunolabeling with mouse anti-gE and rabbit 233 anti-gC antibodies. The representative syncytium at 72 hpi with abundant gE staining demonstrated that VZV had undergone several cycles of replication. In contrast, only a small number of cells stained positively for gC; the above gC-enriched focus represented the original inoculum.

TABLE 1. MotifFinder analysis of VZV ORF4 transactivator protein product

HOX9 activation region	Amino acid position	Sequence	Score
1	275–306	RerViRgeSLiEalesadelltwiKMlaaKnl	1042
2	369–400	fvmiARIaNivvRgsKfveyddiscnvqvlqE	1038

gC/gE ratio was found in both of two independent experiments. Thus, this figure confirmed that all treatments increased the gC/gE ratio over the untreated infected cells. Similar results were obtained when the gC/MCP ratio was assessed under the same conditions of treatment versus no treatment (data not shown). These data also controlled for the random variations in syncytial size common to VZV syncytial analysis.

Effect of HMBA treatment on gC expression in a second strain. As an additional confirmatory experiment, we tested the effect of HMBA treatment on the VZV-MSP strain, using an even lower concentration of the inoculum than in the previous experiments presented above (Fig. 9). When the samples were examined by confocal microscopy, the gC-positive inoculum was clearly visible at 24 hpi and was equivalent between the treated and untreated cultures. However, no newly synthesized gC was visible in the untreated cells at 48 hpi, whereas new gC production was obvious in the HMBA-treated sample. By 72 hpi there was clearly more gC in the treated samples, as demonstrated in the confocal images showing only the gC specific staining (Fig. 9). Thus, the HMBA effect was maintained after infection with different strains.

In order to document that HMBA treatment was increasing HOX levels as predicted by the bioinformatics analysis in Table 2, we investigated whether we could detect HOXA9 protein in untreated or treated cells, using a previously described immunoblotting protocol (43). The MeWo cells were subcultured and incubated for 3 days. At the zero time point, no HOXA9 protein was detected by immunoblotting in uninfected MeWo cells (Fig. 10; lane 1). After incubation for another 48 h, however, the HOXA9 protein was detected in both untreated and treated cells. As expected, the amount of HOXA9 protein was increased substantially in the HMBA-treated monolayers. Densitometric analyses performed when the lesser band (lane 2) first became detectable showed a fivefold increase in the treated sample (lane 3).

DISCUSSION

These results document an unexpected pattern for VZV gC expression that is completely different from the other major VZV glycoproteins and apparently also different from any HSV glycoprotein. In HSV-1 infection, a relatively abundant transcript for the gamma-2 gC is present by 5 hpi (38, 41), and the protein is expressed at high levels within a single HSV replication cycle of about 10 to 14 h (21). The delay in VZV gC expression may explain some of the anomalous and sometimes conflicting findings about VZV gC in the literature. For example, the interesting observation that VZV variants producing no gC arise spontaneously after multiple passages in cell culture and can be isolated by repeated plaque purification may be explained by the results found here (18, 19). In this situation, if a monolayer were inoculated with cells obtained from an infected monolayer before maximal gC production and if this process were repeated multiple times, eventually the newly infected monolayer would exhibit little or no gC expression (even though the virus contained an intact gC gene and still could produce gC if given sufficient incubation time). Similarly, the fact that a gC-negative virus grew to a titer similar to that of a gC-positive virus may need to be reinvestigated under conditions that assure substantial gC production by the gC-positive virus in a particular experiment (4, 18).

Third, whether VZV gC attaches to heparan sulfate has been debated in the literature (4, 37). Again, if the initial cell culture experiments were performed with infected monolayers producing either low or highly variable amounts of gC, the results would appear to indicate that VZV gC lacks the ability to bind heparan sulfate. When we performed CLUSTAL W alignment of VZV gC, based on the heparan sulfate binding data for HSV-1 gC (23), we found that VZV gC had notable homology with the region that is responsible for heparan sulfate binding for HSV gC. Upon subsequent analysis, an Emini surface accessibility algorithm predicted that this HSV-1 gC putative heparan sulfate binding region will overlap a region of the VZV gC ectodomain predicted to have the highest probability of surface accessibility (7). Furthermore, our confocal

TABLE 2. MatInspector analysis of ORF4 and ORF14 promoter *cis* elements[a]

Promoter	Optimized matrix	Position upstream	Similarity		Sequence	Further information
			Core	Matrix		
ORF4						
HOXA9	0.87	120–104	1	0.94	agaag**catt**AATCatgt	HOXA9 homeobox factor
TALE/TGIF	1	21–11	1	1	aatt**GTCA**gat	TG-interacting factor belonging to TALE (e.g., PBX-1)
ORF14						
MEIS1B_HOXA9	0.78	240–226	1	0.92	**TGACt**gt**tttat**ggc	MEIS1b and HOXA9 heterodimer binding target DNA
PBX/HOXA9	0.79	240–224	0.75	0.83	tga**cTGTTtat**ggcat	PBX-HOXA9 binding site
HOXC13	0.91	188–172	1	0.93	attat**aa****TAAA**tctatg	Homeodomain transcription factor HOXC13
TALE/TGIF	1	19–11	1	1	atg**tGTCA**ata	TG-interacting factor belonging to TALE (e.g., PBX1)
HOXC13	0.91	17–1	1	0.91	gtgtc**aa****TAAA**aaccag	Homeodomain transcription factor HOXC13

[a] The matrix similarity is the score of the complete matrix match, whereas the core similarity is the score of the highest conserved positions of a matrix match. In general, a matrix similarity above 0.80 will imply a good match. The sequence includes the conservation index value (ci-value) as determined by a formula described by Cartharius et al. (2). ci-values above 60 are in boldface; capital letters indicate core sequence.

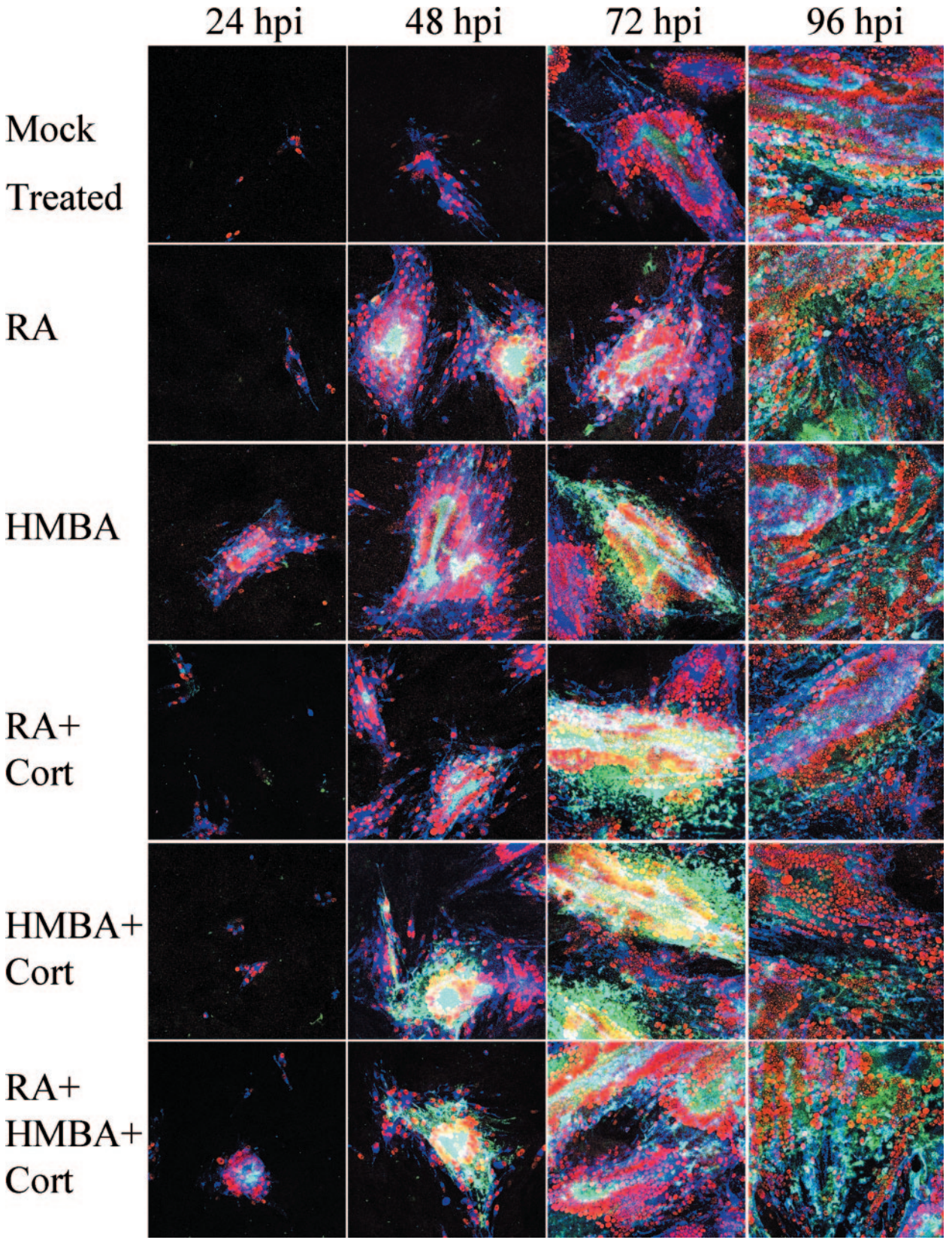

FIG. 7. Enhanced expression of VZV gC after treatment with HMBA, RA, and cortisol. After infection with a sonicated VZV inoculum, Mewo cell monolayers were treated with chemicals known to induce the production of PBX and HOX proteins: RA; HMBA; RA and cortisol; HMBA and cortisol; and RA, HMBA, and cortisol. Fresh medium was added at 0 and 48 hpi, along with the treatments, where indicated. Several hundred micrographs of syncytia in each well at each time point were obtained, from which were prepared Z-stack images of four to five representative syncytia. All settings and conditions were identical between these images and Fig. 6. The antibody reagents were the same as in Fig. 5. Green, gC; blue, gE; red, major capsid protein.

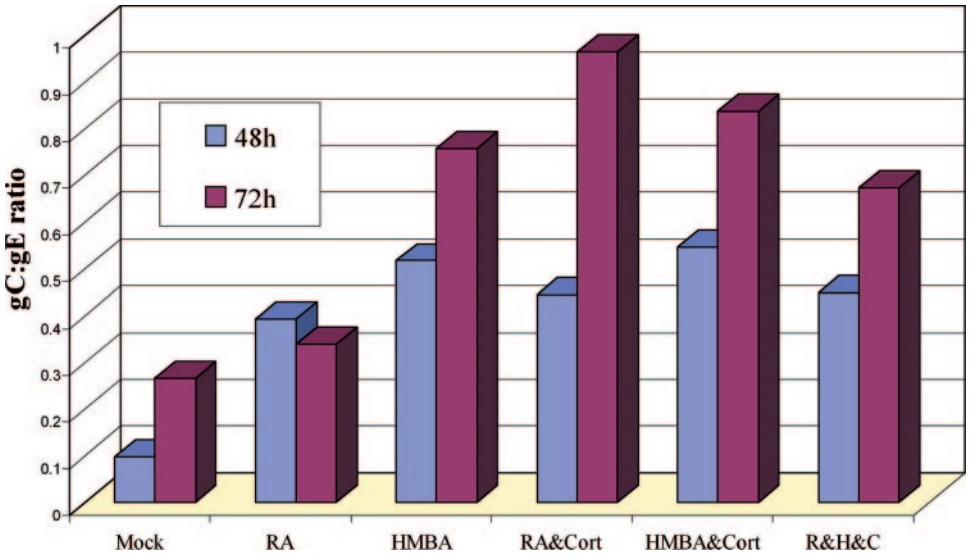

FIG. 8. The gC/gE ratio in VZV-infected cells at 48 and 72 hpi. VZV infections were carried out as described in the legend to Fig. 7, in the presence of one or more of the following three chemicals: HMBA, RA, and cortisol. After immunostaining the cultures with anti-gE and anti-gC antibodies, the pixels were measured within representative syncytia using an ImageJ RGB measure. The ratio of average gC to average gE production was found to increase at both 48 and 72 h postinfection with treated cells. This increase in the gC/gE ratio was found in two independent experiments.

microscopy results indicated that inoculum cells that adhered to the monolayer consisted mainly of gC-positive cells (see Fig. 3 and 9). Thus, the current evidence suggested that VZV gC could possess the capacity to bind heparan sulfate.

These results also address issues about VZV pathogenesis. In the SCID-hu mouse model, low-passage wild-type strains that produce gC induce a productive infection in the skin implant that resembles the pathology in human skin. In contrast, VZV strains lacking gC expression grow poorly after inoculation into human skin implants (25). Furthermore, strains lacking gC expression did not penetrate through the epidermal cell layer of an implant, nor did they form prototypical enveloped virions at the cell surface of the infected implant. Thus, the gC protein is associated with complete virion morphogenesis and skin pathogenesis. When these points are considered together, the delayed production of VZV gC in cell culture may provide at least a partial explanation for the extremely low titer of infectious virus, with the assumption that many viral particles produced during the first three to four replication cycles (12 to 48 hpi) would lack gC in their envelopes. Thus, VZV in cell culture may consist of two populations: those with gC and those with little or no gC.

Another important finding in this gC project was related to an extensive bioinformatics search, namely, that transcription factor binding sites for the PBX/HOX family were found in both the promoter regions of ORF14 and ORF4. PBX was originally identified as a gene involved in embryogenesis and also as a proto-oncogene in some forms of leukemia (33). Subsequent studies determined that PBX acts as a cofactor to HOX proteins. In turn, HOX proteins are homeodomain transcription factors that regulate cell fate decisions during embryogenesis and other differentiation events (33). Based on HSV ICP27 and PRV UL54 protein data (17, 35), we were interested in the mechanism by which ORF4 may upregulate gC in the VZV system. When we analyzed the ORF4 protein for transcription activation related motifs using MotifFinder (default settings), we determined that the ORF4 protein harbored two HOXA9 activation regions (Table 1). When we selected MatInspector to analyze the proximal promoter region of ORF14, we found PBX/HOXA9 and TALE/HOXC13 binding sites (Table 2). MatInspector also identified a HOXA9 binding site upstream of ORF4. Interestingly, HMBA, which induces HOX and PBX expression resulting in cellular differentiation, has been shown to upregulate transcription of the immediate-early ORF4 homolog ICP27 in HSV (45). In VZV, the ORF4 protein is found mainly in the cytoplasm at early times after infection (22). A bidirectional nucleocytoplasmic shuttling signal is important for nuclear localization in late times of infection, when IE4 may exert its transactivator functions, including those potentially involved in gC biosynthesis (1). HMBA has been shown to complement a defect in HSV VP16 (45), which transactivates HSV ICP27 through interaction with its PBX/HOX5 motif, commonly referred to as the TAATGARAT sequence. Thus, VZV gC expression appears to be upregulated by a late HOX protein, whereas HSV is upregulated by an intermediate HOX protein (6, 8, 24).

The presence of PBX/HOX motifs in the promoter region of VZV gC suggests that late HOX proteins play an important role for gC expression in the skin. HOXC13 is expressed primarily in hair follicles and terminally differentiated skin. Similarly, VZV infection is identified by its vesicular skin rash, and these vesicles frequently cluster around hair follicles in human skin (44). Furthermore, VZV replication is inhibited by roscovitine, an inhibitor of cyclin-dependent kinases (42). The mechanism of action of roscovitine has been studied in Moloney murine leukemia virus, which contains a PBX consensus element located in the long terminal repeat known to be important for transcription (3). The addition of roscovitine to retrovirus in-

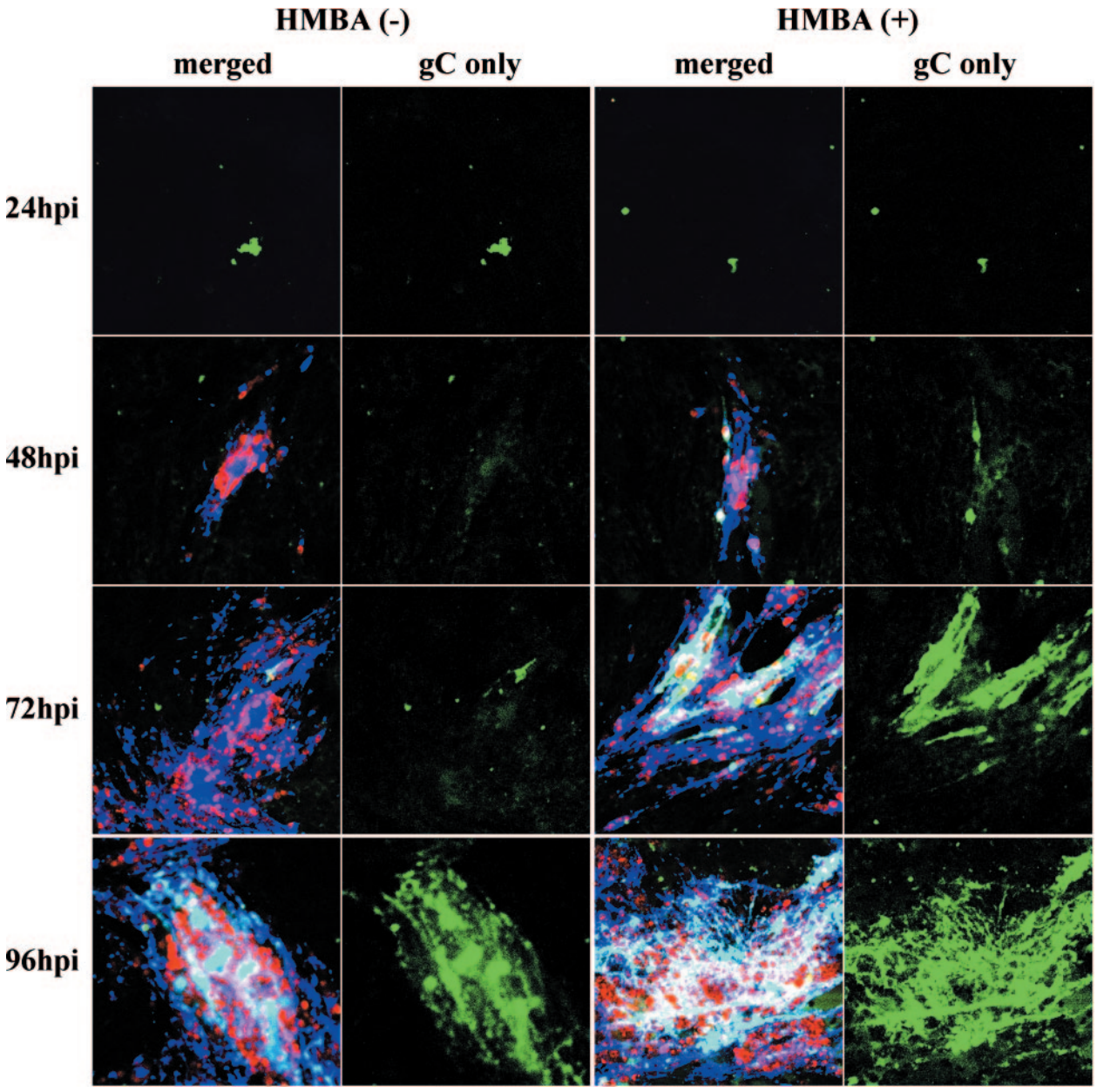

FIG. 9. HMBA treatment of cells infected with a second strain called VZV-MSP. The inoculum was prepared from extensively sonicated monolayers. The infected monolayers were immunolabeled as described in the legends to Fig. 5 and 7, and images were collected using identical confocal microscopy settings. The first and third columns show the merged images of MCP (red), gE (blue), and gC (green), whereas the second and fourth columns show gC alone (green only) at each time point. Note the remnants of VZV gC in the inoculum material bound to the monolayers in the 24-hpi samples.

fected cultures downregulates PBX and markedly inhibits viral transcription (3). Thus, roscovitine may inhibit VZV replication by inhibiting PBX/HOX transcription.

Further circumstantial evidence implicating PBX/HOX involvement in VZV pathogenesis is the extremely well documented association between severe disseminated visceral VZV infection and patients with HOX-expressing leukemias (26). In addition, severe VZV disease is seen in bone marrow transplant recipients (5), patients who often receive corticosteroid treatment (16). Even more suggestive are the peculiar features associated with congenital varicella syndrome (9). VZV alone among the human herpesviruses causes a most unusual fetopathy in pregnant women who contract VZV infection during the first half of gestation. The most prominent stigmata of the fetopathy is foreshortening of the extremities, sometimes called a peg-leg syndrome. This limb anomaly is accompanied by severe scarring around the same extremity. Based on results in the present study, a likely explanation for the fetopathy has emerged for the first time. The development of the extremities occurs in a milieu requiring high levels of PBX, HOXA9, and HOXC13. This milieu can be altered by RA, resulting in defects in limb development that are mediated by PBX and

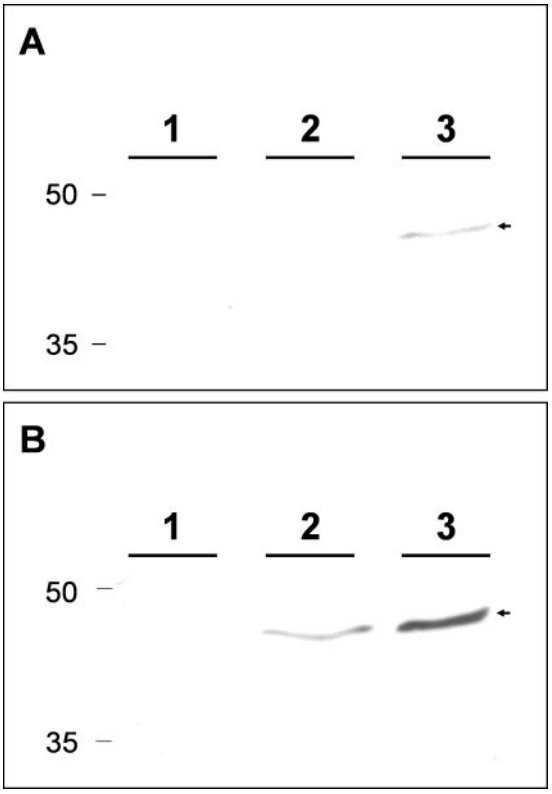

FIG. 10. Detection of HOXA9 protein in MeWo cells. MeWo cell monolayers were passaged and incubated for 3 days. At time zero, one monolayer was harvested (lane 1). Two other monolayers were incubated for an additional 48 h before harvesting; one of these was untreated (lane 2), and one was treated with HMBA (lane 3). Cell lysates were separated on a 12% acrylamide gel and transferred to a polyvinylidene difluoride membrane. All three monolayers were subsequently probed for the HOXA9 protein with a murine MAb. The membrane was exposed for 4 min (A) or 20 min (B). The HOXA9 protein is designated with an arrowhead.

associated homeobox genes (30). In various animal models, the lack of these factors leads to inappropriate limb development. In a human fetus infected with VZV, the normally high PBX/HOX levels in developing extremities would promote persistent viral replication in the same extremities, leading to tissue destruction (scarring) and maldevelopment of the limb. In summary, both laboratory experiments as well as experiments of nature support a role for the PBX/HOX family of transcription factors in regulation of VZV gC biosynthesis.

ACKNOWLEDGMENTS

This research was supported by NIH grant AI22795.

We acknowledge a contribution from the late Edward Wagner. Because of his prior research with HMBA, he critically reviewed our HMBA data during the initial preparation of the manuscript in December 2005.

REFERENCES

1. **Baudoux, L., P. Defechereux, B. Rentier, and J. Piette.** 2000. Gene activation by varicella-zoster virus IE4 protein requires its dimerization and involves both the arginine-rich sequence, the central part, and the carboxyl-terminal cysteine-rich region. J. Biol. Chem. **275:**32822–32831.
2. **Cartharius, K., K. Frech, K. Grote, B. Klocke, M. Haltmeier, A. Klingenhoff, M. Frisch, M. Bayerlein, and T. Werner.** 2005. MatInspector and beyond: promoter analysis based on transcription factor binding sites. Bioinformatics **21:**2933–2942.
3. **Chao, S. H., J. R. Walker, S. K. Chanda, N. S. Gray, and J. S. Caldwell.** 2003. Identification of homeodomain proteins, PBX1 and PREP1, involved in the transcription of murine leukemia virus. Mol. Cell. Biol. **23:**831–841.
4. **Cohen, J. I., and K. E. Seidel.** 1994. Absence of varicella-zoster virus (VZV) glycoprotein V does not alter growth of VZV in vitro or sensitivity to heparin. J. Gen. Virol. **75:**3087–3093.
5. **David, D. S., B. R. Tegtmeier, M. R. O'Donnell, I. B. Paz, and T. M. McCarty.** 1998. Visceral varicella-zoster after bone marrow transplantation: report of a case series and review of the literature. Am. J. Gastroenterol. **93:**810–813.
6. **Douville, P., M. Hagmann, O. Georgiev, and W. Schaffner.** 1995. Positive and negative regulation at the herpes simplex virus ICP4 and ICP0 TAATGARAT motifs. Virology **207:**107–116.
7. **Emini, E. A., J. V. Hughes, D. S. Perlow, and J. Boger.** 1985. Induction of hepatitis A virus-neutralizing antibody by a virus-specific synthetic peptide. J. Virol. **55:**836–839.
8. **Galle, L. E., N. S. Taus, D. J. Maggs, C. P. Moore, and W. J. Mitchell.** 2001. Increased severity of herpes simplex virus type 1-induced keratitis in Hox A5 transgenic mice. Curr. Eye Res. **23:**435–442.
9. **Grose, C.** 1994. Congenital infections caused by varicella-zoster virus and herpes simplex virus. Semin. Pediatr. Neurol. **1:**43–49.
10. **Grose, C.** 1981. Variation on a theme by Fenner: the pathogenesis of chickenpox. Pediatrics **68:**735–737.
11. **Grose, C., D. P. Edwards, W. E. Friedrichs, K. A. Weigle, and W. L. McGuire.** 1983. Monoclonal antibodies against three major glycoproteins of varicella-zoster virus. Infect. Immun. **40:**381–388.
12. **Grose, C., L. Maresova, G. Medigeshi, G. Scott, and G. Thomas.** 2006. Endocytosis of varicella-zoster virus glycoproteins: virion envelopment and egress, p. 155–172. *In* R. Sandri-Goldin (ed.), Alpha herpesviruses: pathogenesis and molecular biology. Horizon Scientific Press, Norfolk, England.
13. **Grose, C., D. M. Perrotta, P. A. Brunell, and G. C. Smith.** 1979. Cell-free varicella-zoster virus in cultured human melanoma cells. J. Gen. Virol. **43:**15–27.
14. **Grose, C., S. Tyler, G. Peters, J. Hiebert, G. M. Stephens, W. T. Ruyechan, W. Jackson, J. Storlie, and G. A. Tipples.** 2004. Complete DNA sequence analyses of the first two varicella-zoster virus glycoprotein E (D150N) mutant viruses found in North America: evolution of genotypes with an accelerated cell spread phenotype. J. Virol. **78:**6799–6807.
15. **Harson, R., and C. Grose.** 1995. Egress of varicella-zoster virus from the melanoma cell: a tropism for the melanocyte. J. Virol. **69:**4994–5010.
16. **Hill, G., A. R. Chauvenet, J. Lovato, and T. W. McLean.** 2005. Recent steroid therapy increases severity of varicella infections in children with acute lymphoblastic leukemia. Pediatrics **116:**e525–e529.
17. **Jean, S., K. M. LeVan, B. Song, M. Levine, and D. M. Knipe.** 2001. Herpes simplex virus 1 ICP27 is required for transcription of two viral late (gamma 2) genes in infected cells. Virology **283:**273–284.
18. **Kinchington, P. R., P. Ling, M. Pensiero, A. Gershon, J. Hay, and W. T. Ruyechan.** 1990. A possible role for glycoprotein gpV in the pathogenesis of varicella-zoster virus. Adv. Exp. Med. Biol. **278:**83–91.
19. **Kinchington, P. R., P. Ling, M. Pensiero, B. Moss, W. T. Ruyechan, and J. Hay.** 1990. The glycoprotein products of varicella-zoster virus gene 14 and their defective accumulation in a vaccine strain (Oka). J. Virol. **64:**4540–4548.
20. **Kinchington, P. R., J. Remenick, J. M. Ostrove, S. E. Straus, W. T. Ruyechan, and J. Hay.** 1986. Putative glycoprotein gene of varicella-zoster virus with variable copy numbers of a 42-base-pair repeat sequence has homology to herpes simplex virus glycoprotein C. J. Virol. **59:**660–668.
21. **Levine, M., A. Krikos, J. C. Glorioso, and F. L. Homa.** 1990. Regulation of expression of the glycoprotein genes of herpes simplex virus type 1 (HSV-1). Adv. Exp. Med. Biol. **278:**151–164.
22. **Lungu, O., C. A. Panagiotidis, P. W. Annunziato, A. A. Gershon, and S. J. Silverstein.** 1998. Aberrant intracellular localization of varicella-zoster virus regulatory proteins during latency. Proc. Natl. Acad. Sci. USA **95:**7080–7085.
23. **Mardberg, K., E. Trybala, J. C. Glorioso, and T. Bergstrom.** 2001. Mutational analysis of the major heparan sulfate-binding domain of herpes simplex virus type 1 glycoprotein C. J. Gen. Virol. **82:**1941–1950.
24. **Mitchell, W., R. De Santo, S. Zhang, W. Odenwald, and H. Arnheiter.** 1993. Herpes simplex virus pathogenesis in transgenic mice is altered by the homeodomain protein Hox 1.3. J. Virol. **67:**4484–4491.
25. **Moffat, J. F., L. Zerboni, P. R. Kinchington, C. Grose, H. Kaneshima, and A. M. Arvin.** 1998. Attenuation of the vaccine Oka strain of varicella-zoster virus and role of glycoprotein C in alphaherpesvirus virulence demonstrated in the SCID-hu mouse. J. Virol. **72:**965–974.
26. **Panagopoulos, I., M. Isaksson, R. Billstrom, B. Strombeck, F. Mitelman, and B. Johansson.** 2003. Fusion of the NUP98 gene and the homeobox gene HOXC13 in acute myeloid leukemia with t(11;12)(p15;q13). Genes Chromosomes Cancer **36:**107–112.
27. **Pasieka, T. J., L. Maresova, K. Shiraki, and C. Grose.** 2004. Regulation of varicella-zoster virus-induced cell-to-cell fusion by the endocytosis-competent glycoproteins gH and gE. J. Virol. **78:**2884–2896.
28. **Perera, L. P., J. D. Mosca, M. Sadeghi-Zadeh, W. T. Ruyechan, and J. Hay.**

1992. The varicella-zoster virus immediate-early protein, IE62, can positively regulate its cognate promoter. Virology **191:**346–354.
29. **Preston, C. M., and M. McFarlane.** 1998. Cytodifferentiating agents affect the replication of herpes simplex virus type 1 in the absence of functional VP16. Virology **249:**418–426.
30. **Qin, P., R. Cimildoro, D. M. Kochhar, K. J. Soprano, and D. R. Soprano.** 2002. PBX, MEIS, and IGF-I are potential mediators of retinoic acid-induced proximodistal limb reduction defects. Teratology **66:**224–234.
31. **Qin, P., J. M. Haberbusch, K. J. Soprano, and D. R. Soprano.** 2004. Retinoic acid regulates the expression of PBX1, PBX2, and PBX3 in P19 cells both transcriptionally and posttranslationally. J. Cell Biochem. **92:**147–163.
32. **Qin, P., J. M. Haberbusch, Z. Zhang, K. J. Soprano, and D. R. Soprano.** 2004. Pre-B cell leukemia transcription factor (PBX) proteins are important mediators for retinoic acid-dependent endodermal and neuronal differentiation of mouse embryonal carcinoma P19 cells. J. Biol. Chem. **279:**16263–16271.
33. **Sagerstrom, C. G.** 2004. PbX marks the spot. Dev. Cell **6:**737–738.
34. **Santos, R. A., J. A. Padilla, C. Hatfield, and C. Grose.** 1998. Antigenic variation of varicella-zoster virus Fc receptor gE: loss of a major B-cell epitope in the ectodomain. Virology **249:**21–31.
35. **Schwartz, J. A., E. E. Brittle, A. E. Reynolds, L. W. Enquist, and S. J. Silverstein.** 2006. UL54-null pseudorabies virus is attenuated in mice but productively infects cells in culture. J. Virol. **80:**769–784.
36. **Shen, W. F., S. Rozenfeld, A. Kwong, L. G. Kom ves, H. J. Lawrence, and C. Largman.** 1999. HOXA9 forms triple complexes with PBX2 and MEIS1 in myeloid cells. Mol. Cell. Biol. **19:**3051–3061.
37. **Shukla, D., and P. G. Spear.** 2001. Herpesviruses and heparan sulfate: an intimate relationship in aid of viral entry. J. Clin. Investig. **108:**503–510.
38. **Stingley, S. W., J. J. G. Ramirez, S. A. Aguilar, K. Simmen, R. M. Sandri-Goldin, P. Ghazal, and E. K. Wagner.** 2000. Global analysis of herpes simplex virus type 1 transcription using an oligonucleotide-based DNA microarray. J. Virol. **74:**9916–9927.
39. **Subramaniam, N., J. Campion, I. Rafter, and S. Okret.** 2003. Cross-talk between glucocorticoid and retinoic acid signals involving glucocorticoid receptor interaction with the homoeodomain protein Pbx1. Biochem. J. **370:**1087–1095.
40. **Sugano, T., T. Tomiyama, Y. Matsumoto, S. Sasaki, T. Kimura, B. Forghani, and Y. Masuho.** 1991. A human monoclonal antibody against varicella-zoster virus glycoprotein III. J. Gen. Virol. **72:**2065–2073.
41. **Swain, M. A., R. W. Peet, and D. A. Galloway.** 1985. Characterization of the gene encoding herpes simplex virus type 2 glycoprotein C and comparison with the type 1 counterpart. J. Virol. **53:**561–569.
42. **Taylor, S. L., P. R. Kinchington, A. Brooks, and J. F. Moffat.** 2004. Roscovitine, a cyclin-dependent kinase inhibitor, prevents replication of varicella-zoster virus. J. Virol. **78:**2853–2862.
43. **Vijapurkar, U., N. Fischbach, W. Shen, C. Brandts, D. Stokoe, H. J. Lawrence, and C. Largman.** 2004. Protein kinase C-mediated phosphorylation of the leukemia-associated HOXA9 protein impairs its DNA binding ability and induces myeloid differentiation. Mol. Cell. Biol. **24:**3827–3837.
44. **Weigle, K. A., and C. Grose.** 1983. Common expression of varicella-zoster viral glycoprotein antigens in vitro and in chickenpox and zoster vesicles. J. Infect. Dis. **148:**630–638.
45. **Yang, W. C., G. V. Devi-Rao, P. Ghazal, E. K. Wagner, and S. J. Triezenberg.** 2002. General and specific alterations in programming of global viral gene expression during infection by VP16 activation-deficient mutants of herpes simplex virus type 1. J. Virol. **76:**12758–12774.